Journal of the
ENGINEERING MECHANICS DIVISION
Proceedings of the American Society of Civil Engineers

FINITE DYNAMIC MODEL FOR INFINITE MEDIA

By John Lysmer,[1] M. ASCE, and Roger L. Kuhlemeyer,[2] A. M. ASCE

INTRODUCTION

The rational approach to analytical studies of sonic flaw detection methods, blast effects, foundation vibrations, and numerous other dynamic problems is to consider them as wave propagation problems in an infinite solid. This approach has two major advantages: (1) The radiation of energy from the excited zone to the far field is properly accounted for; and (2) the concept of infinity is mathematically convenient when the aim is to find closed form analytical solutions for simple homogeneous systems.

For most of the complicated geometrics encountered in practice it is not possible to find closed form solutions and, therefore, it is necessary to resort to numerical methods of the finite difference or discrete mass type. With these methods only a finite number of nodal points can be considered; thus the numerical methods are not directly applicable to infinite systems. A general method through which an infinite system may be approximated by a finite system with a special viscous boundary condition is described herein. The resulting model may be analyzed by ordinary numerical methods but is handled with particular ease by the finite element method.

Examples utilizing the finite model for analysis of steady state foundation vibration problems are presented herein. The results clearly demonstrate: (1) The near equivalence between an infinite half space and the proposed finite model; and (2) the power of the method to analyze previously unsolvable problems.

Note.—Discussion open until January 1, 1970. To extend the closing date one month, a written request must be filed with the Executive Secretary, ASCE. This paper is part of the copyrighted Journal of the Engineering Mechanics Division, Proceedings of the American Society of Civil Engineers, Vol. 95, No. EM4, August, 1969. Manuscript was submitted for review for possible publication on August 1, 1968.

[1]Asst. Prof. of Civ. Engrg., Univ. of Calif., Berkeley, Calif.

[2]Grad. Student, Dept. of Civ. Engrg., Univ. of Calif., Berkeley, Calif., and Staff Engr., Dames and Moore, San Francisco, Calif. (on leave of absence).

PROPOSED MODEL

Fig. 1 shows a typical example of an infinite system. Consider an imaginary convex boundary enclosing all sources of disturbance and all irregular geometrical features. Propagation of energy will occur only from the interior to the exterior region and all energy arriving at the boundary will pass into the exterior region. The effect of the exterior region on the interior region is therefore identical to that of an energy absorbing or nonreflecting boundary. This observation leads directly to the idea of determining the dynamic response of the interior region from a finite model consisting of the interior region subjected to a boundary condition which ensures that all energy arriving at the boundary is absorbed. The writers have investigated different possibilities for expressing this boundary condition analytically and have found that the most promising way is to express it by the conditions

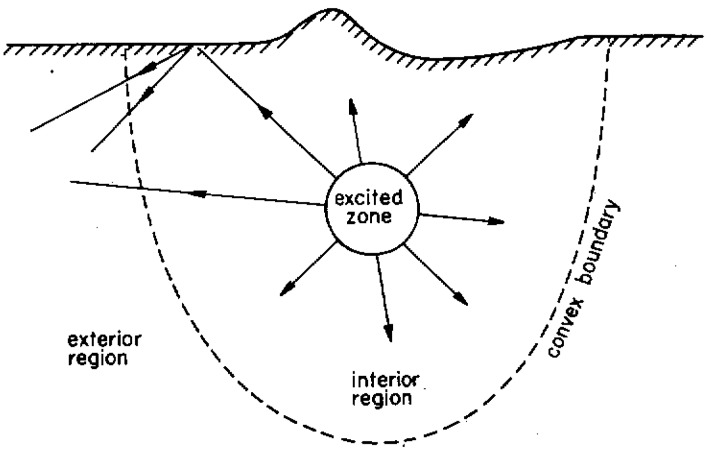

FIG. 1.—TYPICAL INFINITE SYSTEM

$$\sigma = a\,\rho\,V_P\,\dot{w} \qquad (1)$$

$$\tau = b\,\rho\,V_S\,\dot{u} \qquad (2)$$

in which σ and τ are the normal and shear stress, respectively; $\dot{w}$ and $\dot{u}$ are the normal and tangential velocities respectively; ρ is the mass density; V_S and V_P are the velocities of S-waves and P-waves, respectively; and a and b are dimensionless parameters. The proposed boundary condition corresponds to a situation in which the convex boundary is supported on infinitesimal dashpots oriented normal and tangential to the boundary.

REFLECTION AT VISCOUS BOUNDARY

It is necessary to study the reflection of elastic waves at the viscous boundary defined in Eqs. 1 and 2 in order to determine appropriate parameters a and b. The phenomena may be studied by a technique similar to the

one used by Ewing, Jardetzky, and Press (2)[3] for the reflection and refraction of elastic waves at an interface between two media.

Incident P-Wave.—The situation for the case of an incident P-wave is shown in Fig. 2. The x-axis represents the viscous boundary and the elastic medium is located in the lower half plane. The incident wave generates two reflected waves, an S-wave which travels with the velocity

$$V_S = \sqrt{\frac{G}{\rho}} \quad \ldots\ldots\ldots\ldots\ldots\ldots\ldots\ldots\ldots\ldots\ldots\ldots\ldots\ldots\ldots\ldots\ldots\ldots (3)$$

and, a P-wave which propagates with the velocity

$$V_P = \frac{1}{s} V_S \quad \ldots\ldots\ldots\ldots\ldots\ldots\ldots\ldots\ldots\ldots\ldots\ldots\ldots\ldots\ldots\ldots\ldots\ldots (4)$$

In the previous equations G is the shear modulus and s is an elastic constant defined by

$$s^2 = \frac{1 - 2\mu}{2(1 - \mu)} \quad \ldots\ldots\ldots\ldots\ldots\ldots\ldots\ldots\ldots\ldots\ldots\ldots\ldots\ldots\ldots\ldots\ldots\ldots (5)$$

in which μ is Poisson's ratio.

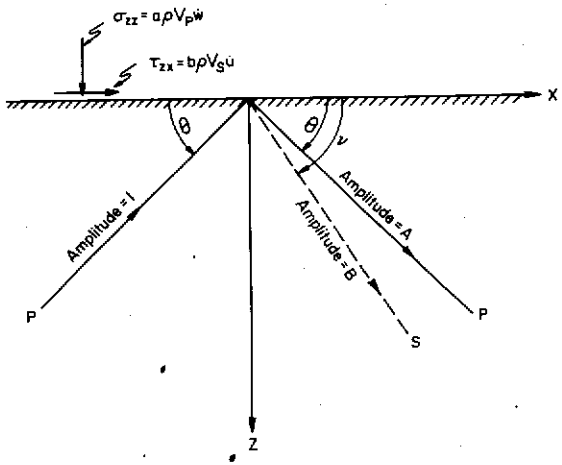

FIG. 2.—INCIDENT P-WAVE AT VISCOUS BOUNDARY

The directions of the incident and reflected waves are related through Snell's Law

$$\cos \nu = s \cdot \cos \theta \quad \ldots\ldots\ldots\ldots\ldots\ldots\ldots\ldots\ldots\ldots\ldots\ldots\ldots\ldots\ldots\ldots\ldots\ldots (6)$$

and the velocity of the wave front along the x-axis is

$$c = V_P \cdot \sec \theta \quad \ldots\ldots\ldots\ldots\ldots\ldots\ldots\ldots\ldots\ldots\ldots\ldots\ldots\ldots\ldots\ldots\ldots\ldots (7)$$

The horizontal and vertical displacements may be written in terms of displacement potentials ϕ and ψ as

[3]Numerals in parentheses refer to corresponding items in the Appendix I.—References.

$$u = \frac{\partial \phi}{\partial x} - \frac{\partial \psi}{\partial z} \quad \ldots \ldots \ldots \ldots \ldots \ldots \ldots \quad (8)$$

$$w = \frac{\partial \phi}{\partial z} + \frac{\partial \psi}{\partial x} \quad \ldots \ldots \ldots \ldots \ldots \ldots \ldots \quad (9)$$

in which $\phi = \phi(x,z,t)$ and $\psi = \psi(x,z,t)$ represent the displacements due to P-waves and S-waves, respectively. Since the wave fronts of the three waves in Fig. 2 must travel along the x-axis at same velocity c, it can be shown that the displacement potentials for harmonic waves of frequency ω must have the form

$$\phi = \underbrace{\exp\left[i\,k(c\,t + z\,\tan\,\theta - x)\right]}_{\text{incident P-wave}} + A\,\underbrace{\exp\left[i\,k(c\,t - z\,\tan\,\theta - x)\right]}_{\text{reflected P-wave}} \quad (10)$$

$$\text{and}\quad \psi = B\,\underbrace{\exp\left[i\,k(c\,t - z\,\tan\,\nu - x)\right]}_{\text{reflected S-wave}} \quad \ldots \ldots \ldots \ldots \quad (11)$$

in which k is the wave number defined by

$$k = \frac{\omega}{c} \quad \ldots \ldots \ldots \ldots \ldots \ldots \ldots \ldots \quad (12)$$

and A and B are the unknown amplitudes of the reflected waves. These ampli-

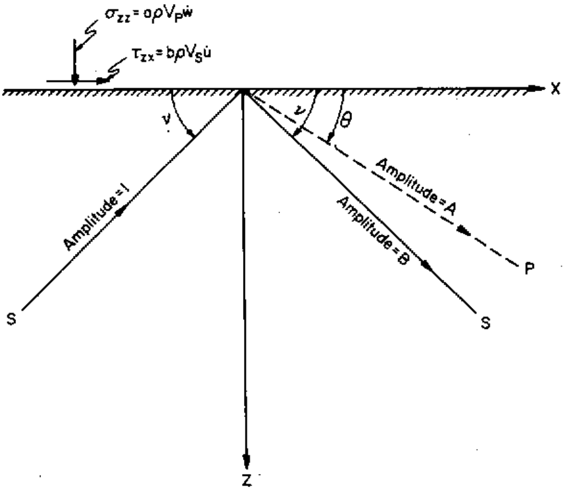

FIG. 3.—INCIDENT S-WAVE AT VISCOUS BOUNDARY

tudes may be determined by the stress boundary conditions defined in Eqs. 1 and 2 which may be expressed in terms of displacement potentials as follows:

$$\frac{1 - 2\,s^2}{s^2}\,\nabla^2\,\phi + 2\left(\frac{\partial^2 \phi}{\partial z^2} + \frac{\partial^2 \psi}{\partial x\,\partial z}\right) = \frac{a}{s\,V_S}\left(\frac{\partial \dot{\phi}}{\partial z} + \frac{\partial \dot{\psi}}{\partial x}\right) \quad \ldots \ldots \quad (13)$$

$$2\frac{\partial^2\phi}{\partial x\,\partial z} + \frac{\partial^2\psi}{\partial x^2} - \frac{\partial^2\psi}{\partial z^2} = \frac{b}{V_S}\left(\frac{\partial\dot{\phi}}{\partial x} - \frac{\partial\dot{\psi}}{\partial z}\right) \quad \ldots\ldots\ldots\ldots\ldots (14)$$

Substitution of Eqs. 10 and 11 into Eqs. 13 and 14 yields the two linear equations

$$(1 - 2s^2\cos^2\theta + a\sin\theta)A + (\sin 2\nu + a\cos\theta)B$$
$$= 2s^2\cos^2\theta - 1 + a\sin\theta \quad \ldots\ldots\ldots\ldots\ldots\ldots\ldots (15)$$

$$(b\cos\nu + s^2\sin 2\theta)A + (\cos 2\nu - b\sin\nu)B$$
$$= s^2\sin 2\theta - b\cos\nu \quad \ldots\ldots\ldots\ldots\ldots\ldots\ldots\ldots (16)$$

from which the amplitudes A and B may be determined as functions of the incident angle θ.

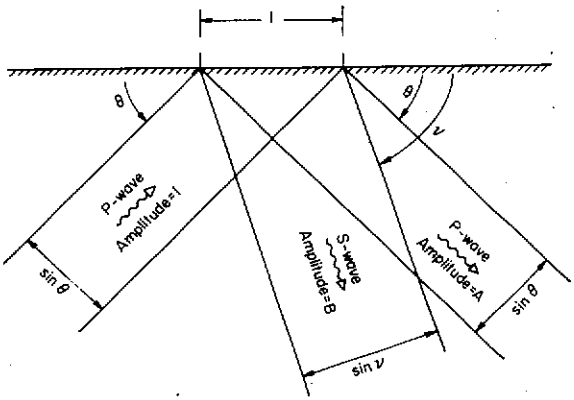

FIG. 4.—INCIDENT P-WAVE

Incident S-Wave.—The case of an incident S-wave shown in Fig. 3 may be solved in a similar fashion. Eqs. 6 to 9 and Eqs. 12 to 14 are valid for this case but Eqs. 10 and 11 must be replaced by

$$\phi = A\exp\underbrace{[ik(ct - z\tan\theta - x)]}_{\text{reflected P-wave}} \quad \ldots\ldots\ldots\ldots\ldots\ldots (17)$$

$$\psi = \underbrace{\exp[ik(ct + z\tan\nu - x)]}_{\text{incident S-wave}} + B\underbrace{\exp[ik(ct - z\tan\nu - x)]}_{\text{reflected S-wave}} \quad (18)$$

Thus the linear equations applicable to define A and B for the case of an incident S-wave are as follows:

$$(s^2\sin 2\theta + b\cos\nu)A + (\cos 2\nu - b\sin\nu)B = -\cos 2\nu - b\sin\nu \quad (19)$$

$$(-\cos 2\nu + a\sin\theta)A + (\sin 2\nu + a\cos\theta)B = \sin 2\nu - a\cos\theta \quad (20)$$

A special case occurs when the incident angle ν becomes smaller than the critical angle ν_{cr} defined by

$$\cos \nu_{cr} = s \quad \ldots\ldots\ldots\ldots\ldots\ldots\ldots\ldots\ldots\ldots\ldots\ldots\ldots\ldots\ldots\ldots\ldots\ldots \quad (21)$$

In this case Eq. 6 yields

$$\cos \theta = \frac{\cos \nu}{s} > 1 \quad \ldots\ldots\ldots\ldots\ldots\ldots\ldots\ldots\ldots\ldots\ldots\ldots\ldots\ldots\ldots\ldots\ldots\ldots \quad (22)$$

$$\sin \theta = -i\sqrt{\cos^2 \theta - 1} \quad \text{(imaginary)} \quad \ldots\ldots\ldots\ldots\ldots\ldots\ldots\ldots\ldots\ldots\ldots\ldots \quad (23)$$

which, upon substitution in Eqs. 19 and 20, leads to complex solutions $A = A_1 + iA_2$ and $B = B_1 + iB_2$ for the amplitudes of the two reflected waves. The physical significance of the complex amplitudes is that a reflected P-wave does not exist and, instead, a wave type similar to a Rayleigh wave appears. This wave, which will be called the boundary wave, travels along the boundary with an amplitude which decreases exponentially with the distance from the boundary.

Energy Considerations.—The purpose of the present investigation is to study the ability of the viscous boundary to absorb impinging elastic waves.

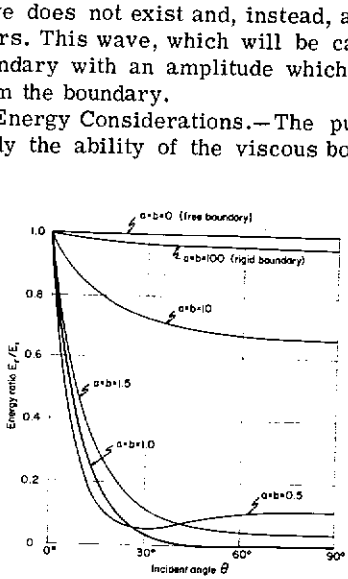

FIG. 5.—ENERGY RATIO FOR INCIDENT P-WAVE

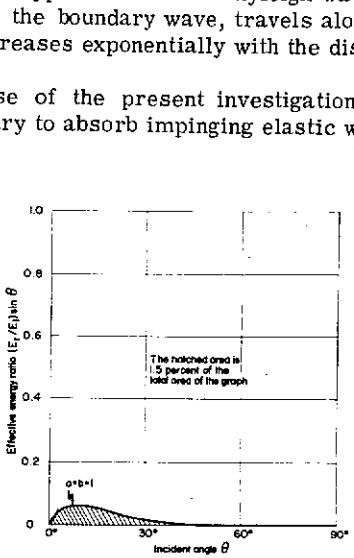

FIG. 6.—EFFECTIVE ENERGY RATIO FOR INCIDENT P-WAVE

A good measure for this ability is the energy ratio defined as the ratio between the transmitted energy of the reflected waves and the transmitted energy of the incident wave. This ratio can be computed from the wave amplitudes A and B by considering the energy flow to and from a unit area of the boundary. The situation for an incident P-wave is shown in Fig. 4. By elementary wave theory it can be shown that the energy transmitted per unit of time through a unit area of the wave front of an S-wave with amplitude B is

$$W_S = \frac{1}{2} \rho V_S \omega^2 B^2 \quad \ldots\ldots\ldots\ldots\ldots\ldots\ldots\ldots\ldots\ldots\ldots\ldots\ldots\ldots\ldots\ldots\ldots\ldots \quad (24)$$

The similar expression for a P-wave with amplitude A is

$$W_P = \frac{1}{2s} \rho V_S \omega^2 A^2 \quad \ldots\ldots\ldots\ldots\ldots\ldots\ldots\ldots\ldots\ldots\ldots\ldots\ldots\ldots\ldots\ldots\ldots\ldots \quad (25)$$

The area of the wave front for the incoming P-wave in Fig. 4 is $\sin \theta$ and the

amplitude is unity. Consequently the incident energy is

$$E_i = \frac{1}{2s} \rho V_S \omega^2 \sin\theta \quad \ldots\ldots\ldots\ldots\ldots\ldots\ldots\ldots\ldots\ldots (26)$$

Similarly, the reflected energy is

$$E_r = \frac{1}{2s} \rho V_S \omega^2 A^2 \sin\theta + \frac{1}{2} \rho V_S \omega^2 B^2 \sin\nu \quad \ldots\ldots\ldots\ldots\ldots\ldots (27)$$

and the energy ratio becomes

$$\frac{E_r}{E_i} = A^2 + s\frac{\sin\nu}{\sin\theta} B^2 \quad \ldots\ldots\ldots\ldots\ldots\ldots\ldots\ldots\ldots\ldots (28)$$

For a given choice of a and b the energy ratio depends only on the incident angle θ and Poisson's ratio μ. The variation of the energy ratio with θ for Poisson's ratio equal to 0.25 is shown in Fig. 5. Other values of Poisson's ratio give similar results. A unit energy ratio corresponds to perfect reflection while a zero energy ratio corresponds to complete absorption. From Fig. 5 it appears that the viscous boundary corresponding to the choice $a = b = 1$ gives maximum absorption. The absorption cannot be made perfect over the whole range of incident angles by any choice of a and b. Fig. 5 shows that nearly perfect absorption is obtained in the range $\theta > 30°$ for $a = b = 1$ while some reflection occurs at smaller angles. Fig. 4 shows that the energy arriving at the unit area of the boundary is proportional to the width $\sin\theta$ of the wave front. Thus only a small part of the wave energy impinging on a given area will arrive under a small angle, and the average of the product $(E_r/E_i)\sin\theta$ is a good measure of the overall ability of the boundary to absorb energy. The product, herein designated the effective energy ratio, is plotted in Fig. 6. The ratio between the area under the curve and the total area of the graph represents the average of reflected to incident energy. Thus Fig. 6 indicates that the viscous boundary defined by $a = b = 1$ is 98.5% effective in absorbing P-waves.

The results for incident S-waves are somewhat similar. The wave diagram

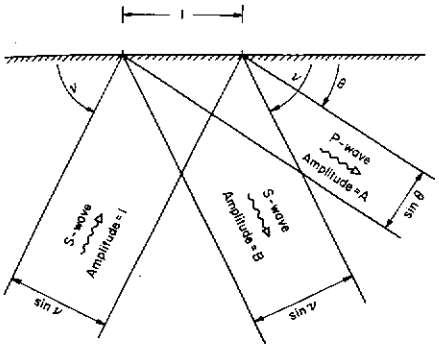

FIG. 7.—INCIDENT S-WAVE

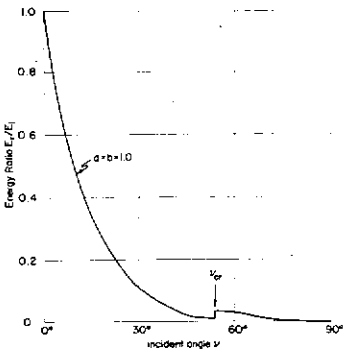

FIG. 8.—ENERGY RATIO FOR INCIDENT S-WAVE

shown in Fig. 7 and Eqs. 24 and 25 give the following counterparts to Eqs. 26 and 27

$$E_i = \frac{1}{2} \rho V_S \omega^2 \sin \nu \quad \ldots\ldots (29)$$

$$E_r = \frac{1}{2} \rho V_S \omega^2 \sin \nu \cdot B^2 + \frac{1}{2s} \rho V_S \omega^2 \sin \theta A^2 \quad \ldots\ldots (30)$$

and the energy ratio becomes

$$\frac{E_r}{E_i} = B^2 + \frac{1}{s} \frac{\sin \theta}{\sin \nu} A^2 \quad \text{for } \nu \geq \nu_{cr} \quad \ldots\ldots (31)$$

This equation is valid only in the region $\nu > \nu_{cr}$. For the subcritical region Eq. 30 must be replaced by

$$E_r = \frac{1}{2} \rho V_S \omega^2 \sin \nu (B_1^2 + B_2^2) \quad \ldots\ldots (32)$$

Eq. 32 does not include energy carried by the boundary wave because this wave transmits no energy to or from the boundary. The energy ratio becomes

$$\frac{E_r}{E_i} = B_1^2 + B_2^2 \quad \text{for } \nu < \nu_{cr} \quad \ldots\ldots (33)$$

The variation of the energy ratio with the angle of incidence for the case $a = b = 1$, and $\mu = 0.25$ is shown in Fig. 8. The curve is similar to Fig. 5 determined for the incident P-wave, and it may be shown that the viscous boundary defined by $a = b = 1$ is 95% effective in absorbing S-waves. It is important to note that the boundary wave has not been accounted for in complete detail, and some irregularities must be expected due to the existence of this wave. A more detailed study has shown that the relative effect of the boundary wave decreases with increasing frequency and increasing length of the boundary.

In summary it has been shown that the viscous boundary defined by

$$\sigma = \rho V_P \dot{w} \quad \ldots\ldots (34)$$

and $$\tau = \rho V_S \dot{u} \quad \ldots\ldots (35)$$

is a nearly perfect absorber of harmonic elastic waves. Because the absorption characteristics are independent of frequency, the boundary can absorb both harmonic and nonharmonic waves. The viscous boundary defined by Eqs. 34 and 35 will be referred to as the standard viscous boundary.

Rayleigh Wave Absorption.—For steady state problems it is possible to design a viscous boundary that can completely absorb Rayleigh waves. The required boundary is similar to the standard viscous boundary defined in Eqs. 1 and 2 except that the parameters a and b vary with the distance from the free surface.

Consider a Rayleigh wave travelling with velocity V_R in the positive x-direction along the surface of the half space shown in Fig. 9. As shown by Ewing, Jardetzky and Press (2), the displacements are

$$u = f(kz) \sin (\omega t - kx) \quad \ldots\ldots (36)$$

$$w = g(kz) \cos (\omega t - kx) \quad \ldots\ldots (37)$$

in which the wave number k is defined by

$$k = \frac{\omega}{V_R} \quad (38)$$

For the special case of a homogeneous half space the functions $f(kz)$ and $g(kz)$ vary as shown in Fig. 10(a). The velocity of the Rayleigh wave may be ex-

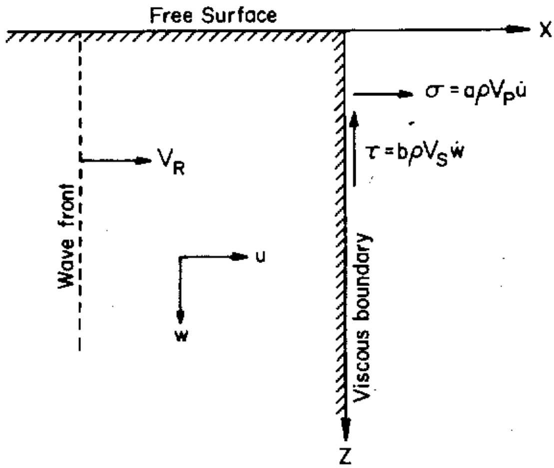

FIG. 9.—RAYLEIGH WAVE ABSORPTION

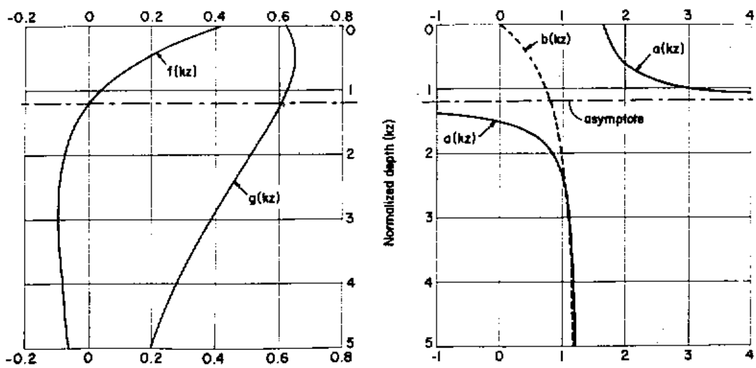

(a) The functions f and g (b) The functions a and b

FIG. 10.—RAYLEIGH WAVE IN HOMOGENEOUS HALF SPACE (μ = 1/4)

pressed as a fraction of V_S by

$$V_R = \frac{V_S}{\eta} \quad (39)$$

The value of η and the functions $f(kz)$ and $g(kz)$ vary with Poisson's ratio. For μ = 1/4 they are η = 1.08766 and

$$f(kz) = D\,[\exp(-0.8475\,kz) - 0.5773\,\exp(-0.3933\,kz)] \quad (40)$$

$$g(kz) = D\,[-0.8475\exp(-0.8475\,kz) + 1.4679\exp(-0.3933\,kz)] \quad \ldots \quad (41)$$

in which D is a constant.

The compressive stress on a vertical plane is

$$\sigma = -(\lambda + 2G)\frac{\partial u}{\partial x} - \lambda\frac{\partial w}{\partial z} \quad \ldots \quad (42)$$

in which $\lambda = 2G\mu/(1 - 2\mu)$ is Lame's constant. Substitution of Eqs. 36 and 37 yields

$$\sigma = k\,[(\lambda + 2G)f(kz) - \lambda g'(kz)]\cos(\omega t - kx) \quad \ldots \quad (43)$$

in which the notation $g'(kz)$ indicates the differentiation, $dg/d(kz)$. Similarly the shear stress on a vertical plane is

$$\tau = -k\,G[f'(kz) + g(kz)]\sin(\omega t - kx) \quad \ldots \quad (44)$$

The particle velocities are by simple differentiation of Eqs. 36 and 37

$$\dot{u} = \omega f(kz)\cos(\omega t - kx) \quad \ldots \quad (45)$$

$$\dot{w} = -\omega g(kz)\sin(\omega t - kx) \quad \ldots \quad (46)$$

Perfect energy absorption will be obtained if Eqs. 1 and 2 are satisfied identically. The required values of a and b may therefore be found by simple substitution of Eqs. 43 to 46 into Eqs. 1 and 2. The result is

$$a(kz) = \frac{1}{\rho V_P}\frac{\sigma}{\dot{u}} = \frac{\eta}{s}\left[1 - (1 - 2s^2)\frac{g'(kz)}{f(kz)}\right] \quad \ldots \quad (47)$$

$$b(kz) = \frac{1}{\rho V_S}\frac{\tau}{\dot{w}} = \eta\left[1 + \frac{f'(kz)}{g(kz)}\right] \quad \ldots \quad (48)$$

The variation of a and b with kz is shown in Fig. 10(*b*). Recognizing that the physical meaning of the variable kz is $2\pi \times$ depth/wavelength it can be seen that at depths greater than one-half wave length the parameters a and b approach constant values. At the depth where the horizontal displacement vanishes the parameter a goes to infinity which agrees with the physical fact that an infinitely viscous dashpot is required to fix a point.

NUMERICAL METHOD

The proposed method has been applied to the foundation vibration problem defined in Fig. 11. The system is axisymmetrical about a vertical axis and consists of a weightless, perfectly rigid, frictionless, circular footing resting on a homogeneous elastic half space. The footing is excited by a vertical harmonic force in the axis of symmetry. This problem has the advantage that an independent solution is available [see Lysmer and Richart (3)] which may be used to check the accuracy of the solution obtained by the method proposed herein.

The vertical displacement δ of the footing is

$$\delta = \frac{P_o}{K} F e^{i\omega t} \quad \ldots \quad (49)$$

in which P_o and ω = the amplitude and frequency, respectively, of the exciting

force; t = time; and K = the static spring constant. It may be shown that

$$K = \frac{4\,G\,r_o}{1-\mu} \quad \ldots\ldots (50)$$

The dimensionless complex quantity $F = F_1 + iF_2$, herein designated the displacement function, is a function of Poisson's ratio μ and the dimensionless frequency ratio a_o defined by

$$a_o = \frac{\omega r_o}{V_S} \quad \ldots\ldots (51)$$

The variation of F_1 and F_2 with a_o is given in Fig. 12 for the case $\mu = 1/3$. The variation of F_1 and F_2 with μ is insignificant.

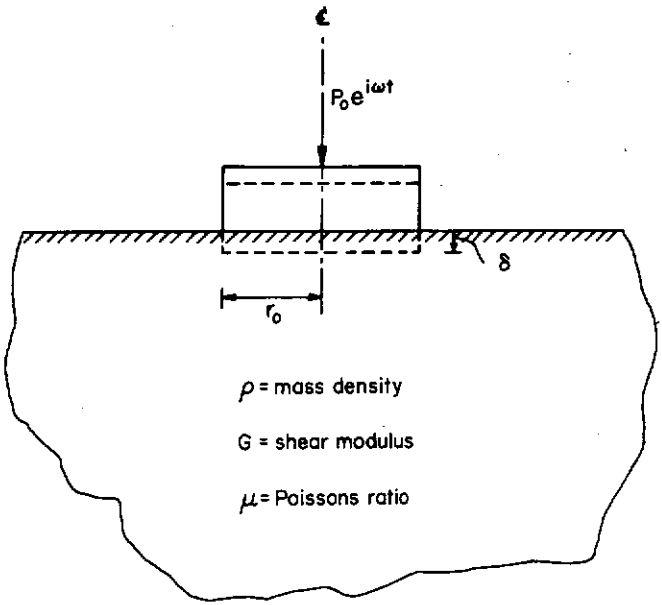

FIG. 11.—FOUNDATION VIBRATION PROBLEM

A finite model of the infinite system was formed by replacing the far field with the standard viscous boundary defined in Eqs. 34 and 35 and is shown in Fig. 13(*a*). The response of the resulting finite system cannot be found by analytical methods but may be approximated by the response of a finite element system of the type shown in Fig. 13(*b*).

Finite Element Method.—The finite element method is an established technique of numerical analysis and only details germane to the problem at hand will be presented herein. The equation of motion for the system in Fig. 13(*b*) is

$$[M]\{\ddot{u}\} + [C]\{\dot{u}\} + [K]\{u\} = \{P\} \quad \ldots\ldots (52)$$

in which $\{u\}$ and $\{P\}$ are the displacement vector and the exciting force vector,

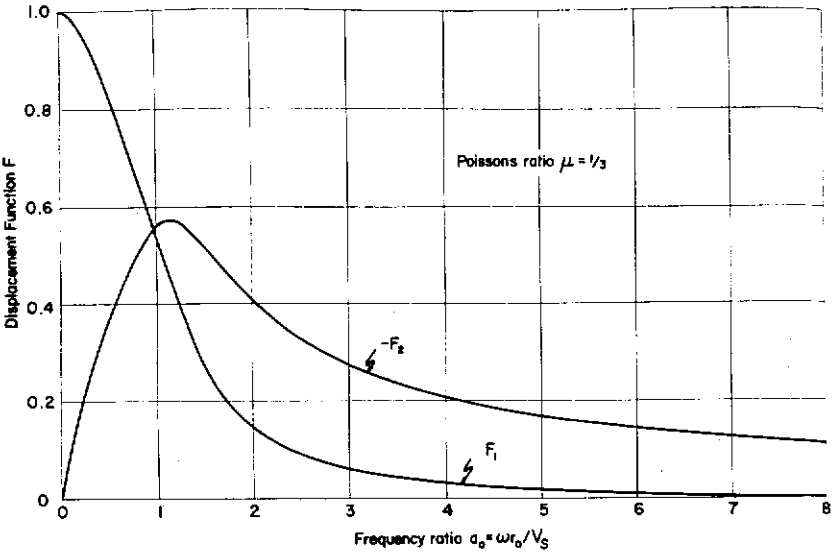

FIG. 12.—DISPLACEMENT FUNCTION FOR RIGID CIRCULAR FOOTING ON ELASTIC HALF SPACE (3)

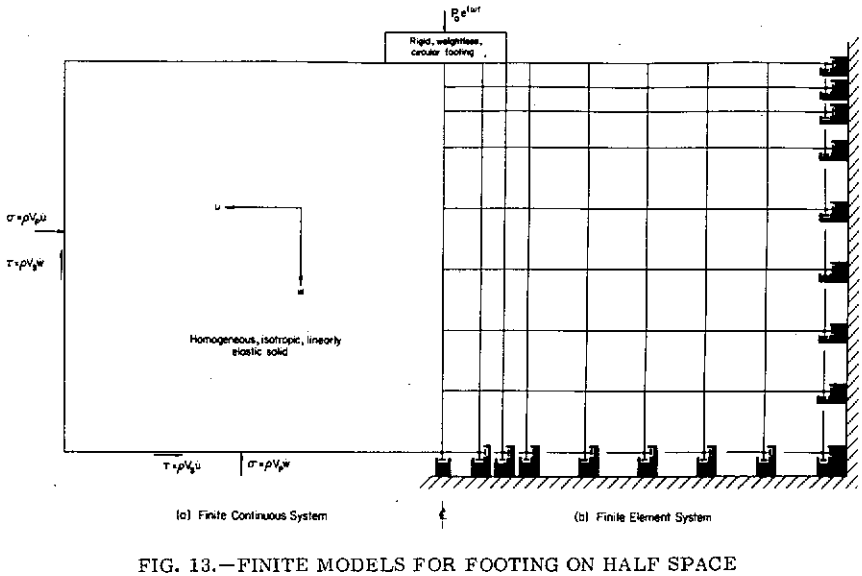

FIG. 13.—FINITE MODELS FOR FOOTING ON HALF SPACE

respectively. Th
at the nodal poin
matrix for the
by standard me
Costantino (1) w
ing the lumped
The solution
complex respon

$$\{P\} = \{P$$

in which $\{P_o\}$ i

$$\{u\} = \{U$$

$$\{\dot{u}\} = i\,\omega$$

and $\{\ddot{u}\} = -\omega$

in which $\{U\}$ i

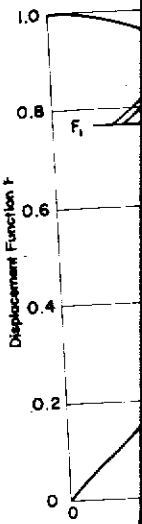

Eqs. 53, 54a
independent

$$[\bar{K}]\{U$$

in which $[\bar{K}$

$$[\bar{K}] =$$

Eq. 55 cons
be solved

respectively. The mass matrix $[M]$ is diagonal because all masses are lumped at the nodal points. The stiffness matrix $[K]$ is identical to the static stiffness matrix for the case where all nodal points are free and may be determined by standard methods. The linear strain rectangular element described by Costantino (1) was used. The damping matrix $[C]$ is a diagonal matrix containing the lumped coefficients for the dashpots on the viscous boundary.

The solution to the steady state problem may be found by the method of complex response. The force vector is

$$\{P\} = \{P_o\} e^{i\omega t} \quad \ldots\ldots (53)$$

in which $\{P_o\}$ is a constant vector. The response is

$$\{u\} = \{U\} e^{i\omega t} \quad \ldots\ldots (54a)$$

$$\{\dot{u}\} = i\,\omega\,\{U\} e^{i\omega t} \quad \ldots\ldots (54b)$$

and $$\{\ddot{u}\} = -\omega^2\,\{U\} e^{i\omega t} \quad \ldots\ldots (54c)$$

in which $\{U\}$ is a constant complex displacement vector. By substitution of

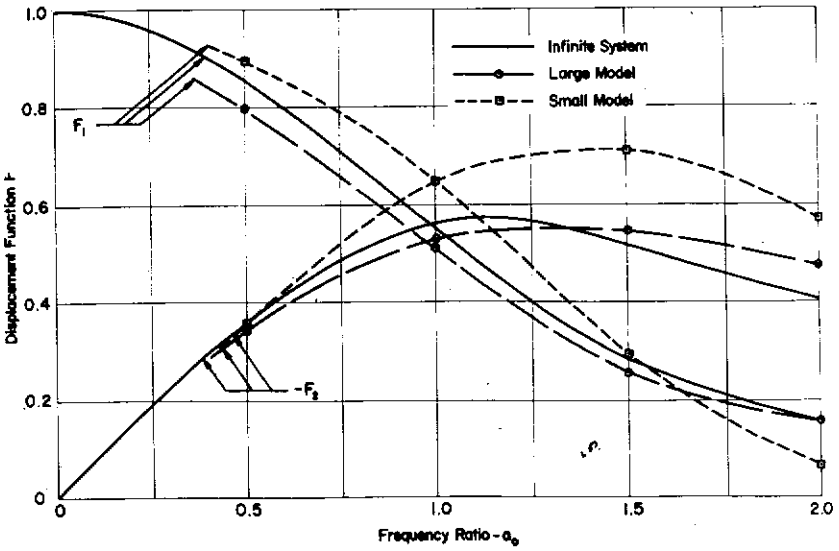

FIG. 14.—RESULTS WITH STANDARD VISCOUS BOUNDARY

Eqs. 53, 54*a*, 54*b*, and 54*c* into Eq. 52 the equation of motion becomes time independent and takes the form

$$[\bar{K}]\{U\} = \{P_o\} \quad \ldots\ldots (55)$$

in which $[\bar{K}]$ is a modified complex stiffness matrix defined by

$$[\bar{K}] = [K] + i\,\omega\,[C] - \omega^2\,[M] \quad \ldots\ldots (56)$$

Eq. 55 constitutes a system of linear equations in complex variables and may be solved for the unknown complex displacements $\{U\}$ by standard methods.

The displacement vector $\{U\}$ contains the footing displacement δ; thus, Eqs. 49 and 50 can be used to compute the real and imaginary parts of the displacement function $F = F_1 + i F_2$ for comparison with the solution for the infinite system.

Choice of Finite Element Mesh.—The accuracy of the finite element method depends on the ratio obtained by dividing the length of the side of the largest element by the minimum wavelength of elastic waves propagating in the system. For accurate results this ratio should be smaller than approximately 1/12. The accuracy depends on the distance from the excited zone to the viscous boundary due to imperfect wave absorption. The error decreases with an increasing ratio between this distance and the minimum wavelength.

The model must be accurate within the operating frequency range for a given problem. From the preceding remarks it is clear that an increase in frequency: (1) Requires a decrease in element size; and (2) allows the over-

TABLE 1.—COMPARISON OF DISPLACEMENT FUNCTIONS FOR SMOOTH AND ROUGH FOOTINGS

a_0	F_1		F_2	
	Smooth footing	Rough footing	Smooth footing	Rough footing
(1)	(2)	(3)	(4)	(5)
0.5	0.8312	0.8089	-0.3688	-0.3533
1.0	0.5593	0.5604	-0.5473	-0.5185
1.5	0.3115	0.3327	-0.5442	-0.5332

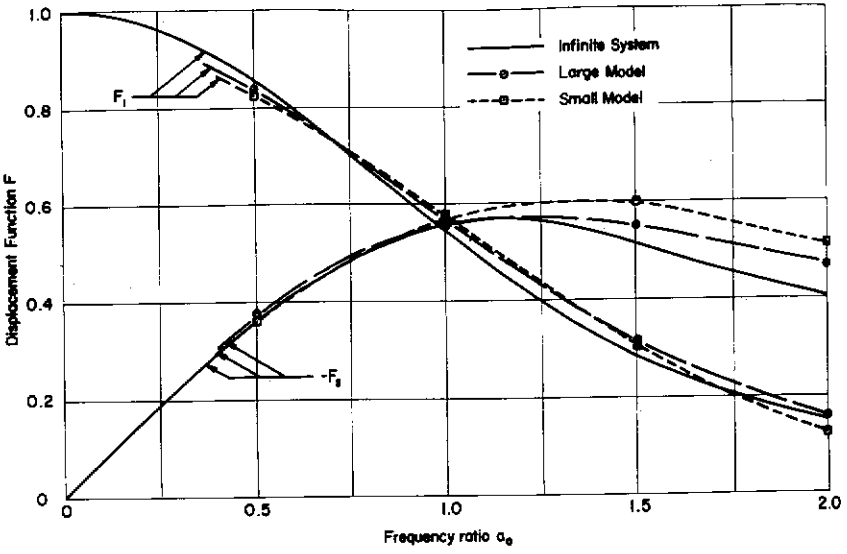

FIG. 15.—RESULTS WITH RAYLEIGH WAVE BOUNDARY

all dimensions of the model to be reduced. These two effects tend to cancel each other; therefore, the accuracy is primarily a function of the total number of nodal points provided the element size is maintained within the subject criterion.

NUMERICAL RESULTS

Numerical results were obtained with two basic models: (1) A small model with 238 nodal points and a distance to the viscous boundary of 3/4 × the wavelength of Rayleigh waves; and (2) a large model with 682 nodal points and a distance to the boundary of 1-1/2 × the wavelength of Rayleigh waves. All calculations were carried out on a CDC 6400 computer. The total processing time required to obtain a value for F at one frequency was 2 min for the small model and 8 min for the large model.

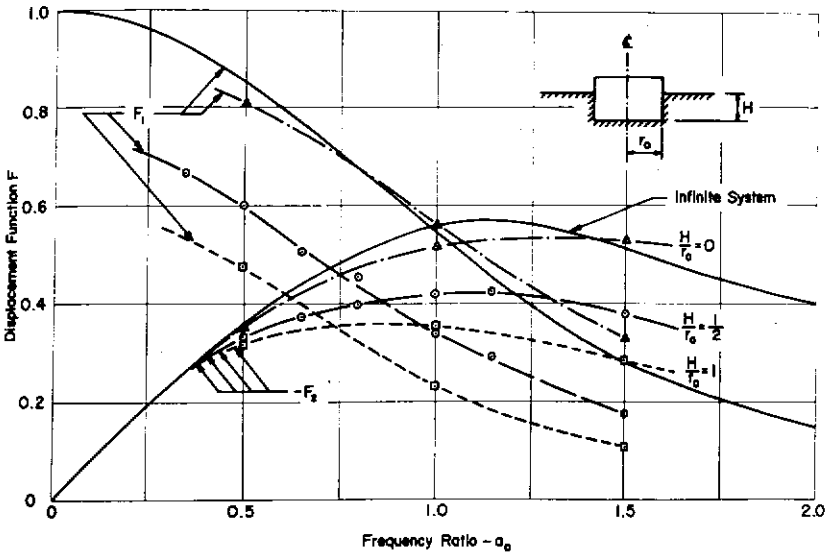

FIG. 16.—RESULTS FOR ROUGH, EMBEDDED FOOTINGS

Comparison with Existing Solution.—Fig. 14 shows a comparison between the displacement function for the infinite system and values obtained utilizing the standard viscous boundary. Good agreement was found when the large model was used while only fair agreement was found for the values obtained by the small model.

A detailed study of the displacement fields obtained with the standard viscous boundary condition revealed minor irregularities caused by a reflected surface wave. The existence of this wave was to be expected because Miller and Pursey (4) have shown that 67% of the energy radiating from a vertically vibrating footing is transmitted in the form of a Rayleigh wave and this type of wave cannot be completely absorbed by the standard viscous boundary. In an attempt to improve the accuracy, the standard viscous boundary on the

vertical face of the model in Fig. 13 was replaced by the Rayleigh wave absorbing boundary defined in Eqs. 47 and 48. The results of calculations based on this model are shown in Fig. 15, and indicates a significant gain in accuracy over the results obtained with the standard viscous boundary. It is proposed, therefore, that the Rayleigh wave boundary be used for all steady state half space problems. The Rayleigh wave boundary cannot be used for transient problems since it is frequency dependent.

Rough Versus Frictionless Footings.—The displacement function shown in Fig. 12 was derived on the assumption of a frictionless surface between the footing and the half space. Because most footings are poured directly on the ground it is of interest to study the effect of the introduction of a rough interface. This is easily accomplished by the finite element method and Table 1 shows the small difference between the displacement functions for a rough

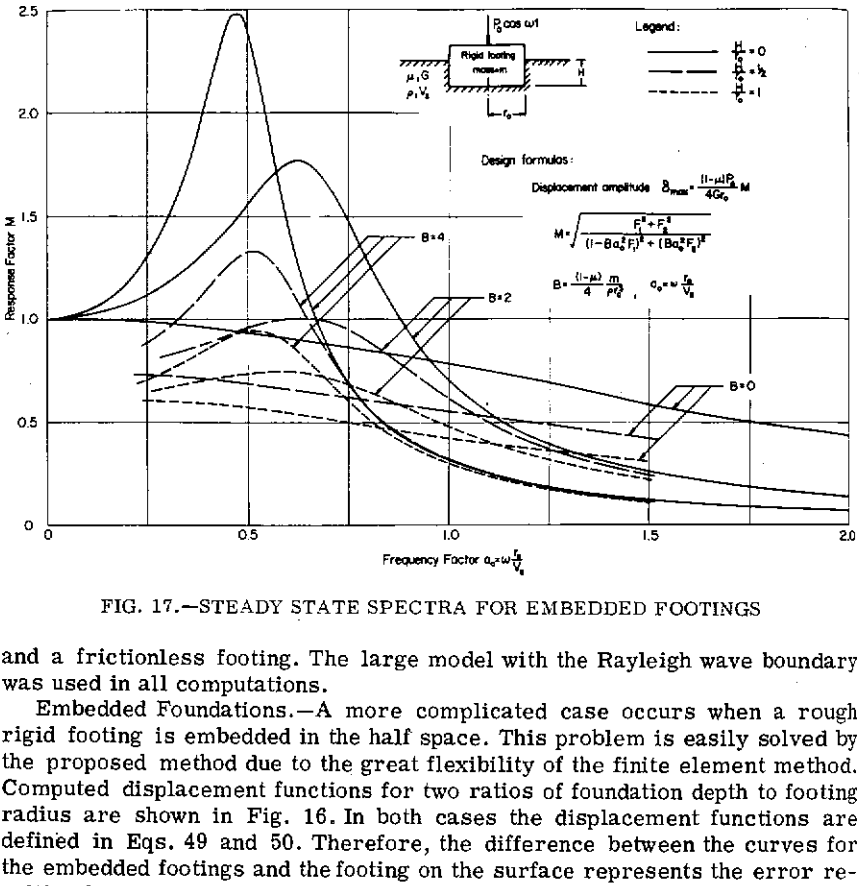

FIG. 17.—STEADY STATE SPECTRA FOR EMBEDDED FOOTINGS

and a frictionless footing. The large model with the Rayleigh wave boundary was used in all computations.

Embedded Foundations.—A more complicated case occurs when a rough rigid footing is embedded in the half space. This problem is easily solved by the proposed method due to the great flexibility of the finite element method. Computed displacement functions for two ratios of foundation depth to footing radius are shown in Fig. 16. In both cases the displacement functions are defined in Eqs. 49 and 50. Therefore, the difference between the curves for the embedded footings and the footing on the surface represents the error resulting from applying the theory for footings on the surface to embedded footings. The large model and the Rayleigh wave boundary condition were used in all computations.

It is convenient for design usage to present the preceding results in the form of response curves reflecting the effect of the mass of the footing. As shown by Lysmer and Richart (3) the displacement of a footing with mass m is

$$\delta = \frac{P_o}{K} \frac{F}{1 - B a_o^2 F} e^{i\omega t} \quad \ldots\ldots\ldots\ldots\ldots\ldots\ldots\ldots\ldots\ldots\ldots\ldots (57)$$

in which B = the mass ratio defined by

$$B = \frac{1 - \mu}{4} \cdot \frac{m}{\rho r_o^3} \quad \ldots\ldots\ldots\ldots\ldots\ldots\ldots\ldots\ldots\ldots\ldots\ldots (58)$$

and K is defined in Eq. 50.

The displacement amplitude is

$$\delta_{max} = \frac{P_o}{K} M \quad \ldots\ldots\ldots\ldots\ldots\ldots\ldots\ldots\ldots\ldots\ldots\ldots (59)$$

in which M = the response factor, expressed as

$$M = \left| \frac{F}{1 - B a_o^2 F} \right| = \sqrt{\frac{F_1^2 + F_2^2}{(1 - B a_o^2 F_1)^2 + (B a_o^2 F_2)^2}} \quad \ldots\ldots (60)$$

Design curves based on values of F_1 and F_2 obtained from Fig. 16 are presented in Fig. 17.

CONCLUSIONS

A numerical method for the analysis of dynamic problems involving infinite continuous systems has been presented. Results obtained by the proposed method show excellent agreement with available theoretical results for an axisymmetrical foundation vibration problem. Two previously unsolvable problems analyzed by the new method were: (1) The effect of friction between a vibrating footing and its foundation; and (2) the effect of embedment of a vibrating footing into the subsoil. The latter effect is quite pronounced and a set of response curves for design use are presented.

The analytical method described has applications far beyond the simple cases presented herein. It may be applied to any infinite system for which all disturbances and irregular geometrical features are limited to a small region of an otherwise homogeneous and linearly elastic space. The irregular zone need not be linear and the exciting forces need not be harmonic; they should have a vanishing time average, however, because the viscous boundary cannot support a static load. Problems involving nonlinearities and transient loads obviously cannot be handled by the method of complex vectors used in this paper but they may be solved by step-by-step procedures.

Only elastic solids have been considered in this paper, but with some modification, it should be possible to adapt the proposed method for the analysis of the near field around antennae and acoustic generators.

ACKNOWLEDGMENTS

The National Science Foundation provided the financial support for this investigation through the Research Initiation Grant No. NSF-GK-1467 to the

University of California at Berkeley. The writers are grateful for this support. All computations were performed on the CDC 6400 digital computer at the University of California at Berkeley.

APPENDIX I.—REFERENCES

1. Costantino, C. J., "Finite Element Approach to Stress Wave Problems," *Journal of the Engineering Mechanics Division*, ASCE, Vol. 93, No. EM2, Proc. Paper 5206, April, 1967, pp. 153–176.
2. Ewing, W. M., Jardetzky, W. S., Press, F., *Elastic Waves in Layered Media*, McGraw-Hill, New York, 1957.
3. Lysmer, J., and Richart, F. E., Jr., "Dynamic Response of Footings to Vertical Loading," *Journal of the Soil Mechanics and Foundations Division*, ASCE, Vol. 92, No. SM1, Proc. Paper 4592, January, 1966, pp. 65–91.
4. Miller, G. F., and Pursey, H., "On the Partition of Energy Between Elastic Waves in a Semi-Infinite Solid," *Proceedings, Royal Society of London*, Series A, Vol. 233, 1955, pp. 55–59.

APPENDIX II.—NOTATION

The following symbols are used in this paper:

A = amplitude of reflected P-wave (see Fig. 2);
A_1, A_2 = real and imaginary parts of A;
a = dimensionless viscous coefficient related to normal stress (see Eq. 1);
a_o = frequency ratio (see Eq. 51);
B = amplitude of reflected S-wave (see Fig. 2), or mass ratio (see Eq. 58);
B_1, B_2 = real and imaginary parts of B;
b = dimensionless viscous coefficient related to shear stresses (see Eq. 2);
$[C]$ = damping matrix (see Eq. 52);
c = velocity of wave front along boundary (see Eq. 7);
D = arbitrary constant (see Eq. 40);
E_i = energy of incident waves (see Eq. 26);
E_r = energy of reflected waves (see Eq. 27);
e = 2.718 . . . = base of natural logarithm;
F = displacement function (see Eq. 49);
F_1, F_2 = real and imaginary parts of F;
$f(kz)$ = amplitude function for the horizontal component of Rayleigh wave (see Eq. 36);
G = shear modulus;
$g(kz)$ = amplitude function for the vertical component of Rayleigh wave (see Eq. 37);
H = depth of embedment (see Fig. 17);
i =
K =
$[K]$ =
$[\bar{K}]$ =
k =
M =
$[M]$ =
m =
$\{P\}$ =
P_o =
$\{P_o\}$ =
r_o =
s =
t =
$\{U\}$ =
$u, \dot{u}$ =
$\{u\}, \{\dot{u}\}, \{\ddot{u}\}$ =
V_P =
V_R =
V_S =
W_P =
W_S =
$w, \dot{w}$ =
x =
z =
δ =
$\delta_{\max}$ =
η =
θ =
λ =
μ =
ν =
ν_{cr} =
π =
ρ =
σ =
τ =
ϕ =
ψ =
ω =

i = imaginary unit;
K = spring constant (see Eq. 50);
$[K]$ = stiffness matrix (see Eq. 52);
$[\bar{K}]$ = modified complex stiffness matrix (see Eq. 56);
k = wave number (see Eqs. 12 and 38);
M = response factor (see Eq. 60);
$[M]$ = mass matrix (see Eq. 52);
m = mass of footing (see Fig. 17);
$\{P\}$ = force vector, time dependent (see Eq. 52);
P_o = amplitude of harmonic force on footing (see Fig. 11);
$\{P_o\}$ = force vector, time independent (see Eq. 53);
r_o = radius of footing (see Fig. 11);
s = ratio between the velocities of S-waves and P-waves (see Eq. 5);
t = time;
$\{U\}$ = displacement vector, time independent (see Eq. 54);
$u, \dot{u}$ = displacement and velocity in x-direction;
$\{u\}, \{\dot{u}\}, \{\ddot{u}\}$ = displacement, velocity and acceleration vector (see Eq. 52);
V_P = velocity of P-waves (see Eq. 4);
V_R = velocity of Rayleigh waves (see Eq. 39);
V_S = velocity of S-waves (see Eq. 3);
W_P = intensity of P-waves (see Eq. 25);
W_S = intensity of S-waves (see Eq. 24);
$w, \dot{w}$ = displacement and velocity in z-direction;
x = horizontal coordinate;
z = vertical coordinate;
δ = complex vertical displacement of footing (see Eq. 49);
$\delta_{\max}$ = absolute value of δ = amplitude (see Eq. 59);
η = ratio between velocities of S-waves and Rayleigh waves (see Eq. 39);
θ = angle between P-wave ray and boundary (see Fig. 2);
λ = Lame's constant (see Eq. 42);
μ = Poisson's ratio;
ν = angle between S-wave ray and boundary (see Fig. 3);
ν_{cr} = critical value of ν (see Eq. 21);
π = 3.1416 . . . ;
ρ = mass density;
σ = normal stress;
τ = shear stress;
ϕ = wave potential for P-waves (see Eq. 8);
ψ = wave potential for S-waves (see Eq. 9); and
ω = circular frequency.